Short-Rib Polydactyly and Jeune Syndromes Are Caused by Mutations in *WDR60*

Aideen M. McInerney-Leo,[1,7] Miriam Schmidts,[2,7] Claudio R. Cortés,[3,7] Paul J. Leo,[1] Blanca Gener,[4] Andrew D. Courtney,[3] Brooke Gardiner,[1] Jessica A. Harris,[1] Yeping Lu,[2] Mhairi Marshall,[1] UK10K Consortium, Peter J. Scambler,[2] Philip L. Beales,[2] Matthew A. Brown,[1] Andreas Zankl,[5,*] Hannah M. Mitchison,[2,8] Emma L. Duncan,[1,6,8] and Carol Wicking[3,8]

Short-rib polydactyly syndromes (SRPS I–V) are a group of lethal congenital disorders characterized by shortening of the ribs and long bones, polydactyly, and a range of extraskeletal phenotypes. A number of other disorders in this grouping, including Jeune and Ellis-van Creveld syndromes, have an overlapping but generally milder phenotype. Collectively, these short-rib dysplasias (with or without polydactyly) share a common underlying defect in primary cilium function and form a subset of the ciliopathy disease spectrum. By using whole-exome capture and massive parallel sequencing of DNA from an affected Australian individual with SRPS type III, we detected two novel heterozygous mutations in *WDR60*, a relatively uncharacterized gene. These mutations segregated appropriately in the unaffected parents and another affected family member, confirming compound heterozygosity, and both were predicted to have a damaging effect on the protein. Analysis of an additional 54 skeletal ciliopathy exomes identified compound heterozygous mutations in *WDR60* in a Spanish individual with Jeune syndrome of relatively mild presentation. Of note, these two families share one novel *WDR60* missense mutation, although haplotype analysis suggested no shared ancestry. We further show that WDR60 localizes at the base of the primary cilium in wild-type human chondrocytes, and analysis of fibroblasts from affected individuals revealed a defect in ciliogenesis and aberrant accumulation of the GLI2 transcription factor at the centrosome or basal body in the absence of an obvious axoneme. These findings show that *WDR60* mutations can cause skeletal ciliopathies and suggest a role for WDR60 in ciliogenesis.

Ciliopathies form an expanding class of heterogeneous congenital diseases mechanistically linked by an underlying dysfunction of the primary cilium (reviewed in Waters and Beales,[1] Hildebrandt et al.,[2] and Lee and Gleeson[3]). This microtubule-based cellular extension is present on virtually all vertebrate cell types during quiescence and has been linked to a number of pivotal developmental signaling pathways, most notably the hedgehog cascade.[4] The cellular anchor of the cilium is the basal body, which derives from the mother centriole and nucleates the axonemal extension.

Ciliopathies are variably characterized by anomalies affecting most major organs and encompass diseases such as polycystic kidney disease and Bardet-Biedl, Joubert, and Meckel syndromes. Within the ciliopathies, a subgroup of disorders including short-rib polydactyly syndrome (SPRS), Jeune syndrome or asphyxiating thoracic dystrophy (JATD [MIM 208500]), Ellis-van Creveld syndrome (EVC [MIM 225500]), and Sensenbrenner syndrome or cranioectodermal dysplasia (CED [MIM 218330]) are characterized by skeletal abnormalities including a small rib cage, shortening of the long bones, and in some cases, polydactyly.[5–7] The severe SRPS class is further divided into five subtypes, namely type I (Saldino-Noonan syndrome [MIM 263530]), type II (Majewski syndrome [MIM 263520]), type III (Verma-Naumoff syndrome [MIM 263510]), type IV (Beemer-Langer syndrome [MIM 269860]), and the recently recognized type V (MIM 614091).[8] Among the skeletal ciliopathies, the SRPS subtypes are the most severe and are incompatible with postnatal life. Skeletal ciliopathies may also manifest extraskeletal phenotypes including polycystic kidney disease, retinal degeneration, and cardiac, liver, and brain anomalies.

To date many mutations causing skeletal ciliopathies affect genes encoding components of the intraflagellar transport (IFT) machinery, a motor-driven trafficking process responsible for transporting proteins required for cilia assembly and function along the axoneme.[9] Transport in the anterograde direction, toward the cilia tip, is mediated by the kinesin-2 motor and a complex of proteins known as IFT-B; opposing retrograde trafficking relies on the dynein-2 motor and the IFT-A complex, although recent evidence suggests that IFT-A proteins are also involved in regulating anterograde trafficking.[10] With the exception of *IFT80* (MIM 611177) mutations in Jeune syndrome[11] and SRPS type III,[12] most skeletal ciliopathies are caused by mutations in genes encoding IFT-A proteins or the

[1]The University of Queensland Diamantina Institute, Translational Research Institute, Level 7, 37 Kent Street, Woolloongabba, QLD 4102, Australia; [2]Molecular Medicine Unit and Birth Defects Research Centre, Institute of Child Health, University College London (UCL), London WC1N 1EH, UK; [3]Institute for Molecular Bioscience, The University of Queensland, St Lucia, QLD 4072, Australia; [4]Servicio de Genética, BioCruces Health Research Institute, Hospital Universitario Cruces, Plaza de Cruces S/N 48903, Barakaldo, Bizkaia, Spain; [5]The University of Queensland, UQ Centre for Clinical Research, Herston, QLD 4029, Australia; [6]Department of Endocrinology, James Mayne Building, Royal Brisbane and Women's Hospital, Butterfield Road, Herston, QLD 4029, Australia
[7]These authors contributed equally to this work
[8]These authors contributed equally to this work
*Correspondence: a.zankl@uq.edu.au
http://dx.doi.org/10.1016/j.ajhg.2013.06.022.

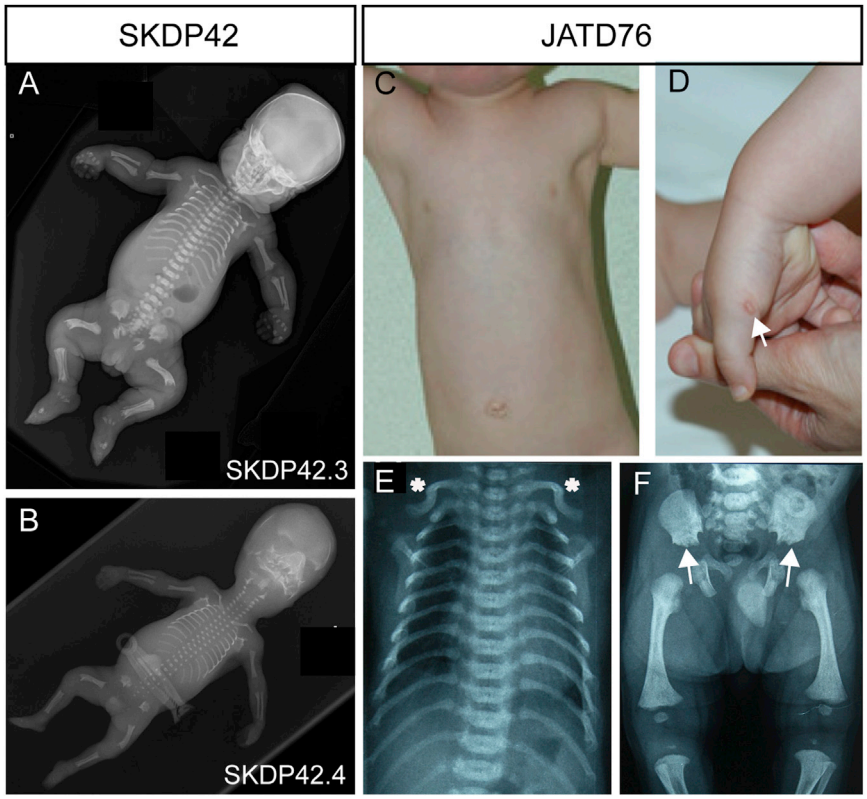

Figure 1. Clinical Features of Individuals from the SRP and Jeune Syndrome Families

(A and B) X-rays of individuals (A) SKDP42.3 (II-1 in Figure 2A) and (B) SKDP42.4 (II-2 in Figure 2A), showing shortening of the ribs and long bones and bowing of the limbs.

(C–F) Individual JATD76 (II-1 in Figure 2A) displays typical hallmarks of Jeune syndrome: mildly narrowed thorax (C), also shown in (E); polydactyly (D, arrow points to remnants of an extra digit subsequently removed from the right hand); handlebar clavicles (E, asterisks); and acetabular spurs (F, arrows).

retrograde IFT motor protein DYNC2H1.[8,13–21] Non-IFT genes implicated in skeletal ciliopathies include *NEK1* (MIM 604588) in SRPS type II[22] and *EVC1* (MIM 604831) and *EVC2* (MIM 607261) in EVC.[23]

Recent advances in massive parallel sequencing technologies offer the opportunity to identify disease-causing mutations for Mendelian disorders in small families previously refractory to classical linkage mapping approaches. With many ciliopathy cases still unresolved at the molecular level and more than 1,000 proteins in the ciliary proteome, this approach is likely to extend the repertoire of genes mutated in ciliopathies. Here we report the use of exome capture and massive parallel sequencing to identify mutations in *WDR60,* a relatively uncharacterized gene, in two separate families with SRPS and Jeune syndrome, respectively.

The first family is a nonconsanguineous Australian family of predominantly British but also Maori descent, with healthy parents and two affected individuals with SRPS type III (Figures 1A and 1B). Individual SKDP42.3 (II-1 in Figure 2A) presented with short long bones on ultrasound at 16 weeks' gestation. Follow-up ultrasound at 31 weeks demonstrated polyhydramnios, severe shortening of long bones with bowed femurs, macrocephaly, short ribs, and ambiguous genitalia. The baby was born at 32 weeks' gestation but died at 2 hr of age. Autopsy confirmed the above findings, and in addition revealed postaxial polydactyly of both hands, syndactyly of some fingers and toes, acetubular spurs, pancreatic fibrosis, mild dilatation of renal tubules, and enlarged liver with ductal plate malformation.

The second affected individual from this family (SKDP42.4; II-2 in Figure 2A) had an unremarkable ultrasound scan at 13 weeks' gestation but demonstrated short ribs and short bowed limbs on ultrasound scan at 17 weeks' gestation. The pregnancy was terminated at this stage. Autopsy further revealed brachydactyly (not polydactyly), conical epiphyses, hypoplastic trabecular, depressed nasal bridge, ventricular septal defect (VSD), focal cystic changes in the kidneys, prominent bile duct plates, and early evidence of pulmonary hypoplasia. Parents did not consent to autopsy of the brain.

With University of Queensland ethics approval (#2011000876) and informed consent, whole-exome sequencing was performed on genomic DNA from individual SKDP42.3 (II-1 in Figure 2A). Sequencing libraries were constructed with the Illumina TruSeqDNA sample preparation kit, combined in pools of six for target capture by the Illumina TruSeq Exome Enrichment Kit, and assessed pre- and postcapture for quality and yield with the Agilent High Sensitivity DNA assay and KAPA Library Quantification Kit. Massive parallel sequencing was performed with six samples per flow cell lane via the Illumina HiSeq2000 platform and version 2 SBS reagents to generate 100 bp paired-end reads. After demultiplexing, the Illumina Data Analysis Pipeline software (CASAVA v.1.8.2) was used for initial base calling. Sequence data were aligned to the current build of the human genome (UCSC Genome Browser, hg19, released February 2009) via the Novoalign alignment tool (v.2.08.02 1);[24] sequence alignment files were converted by SAMtools (v.0.1.14)[25] and Picard tools (v.1.42) (see Table S1 available online for mapping, coverage, and base calling statistics). SNPs and indels were called with the Genome Analysis Toolkit (GATK v.5506)[26,27] and annotated by ANNOVAR.[28]

Further analysis of sequence data was performed with custom scripts employing R and Bioconductor. We retained good-quality SNPs and indels (minimum depth of

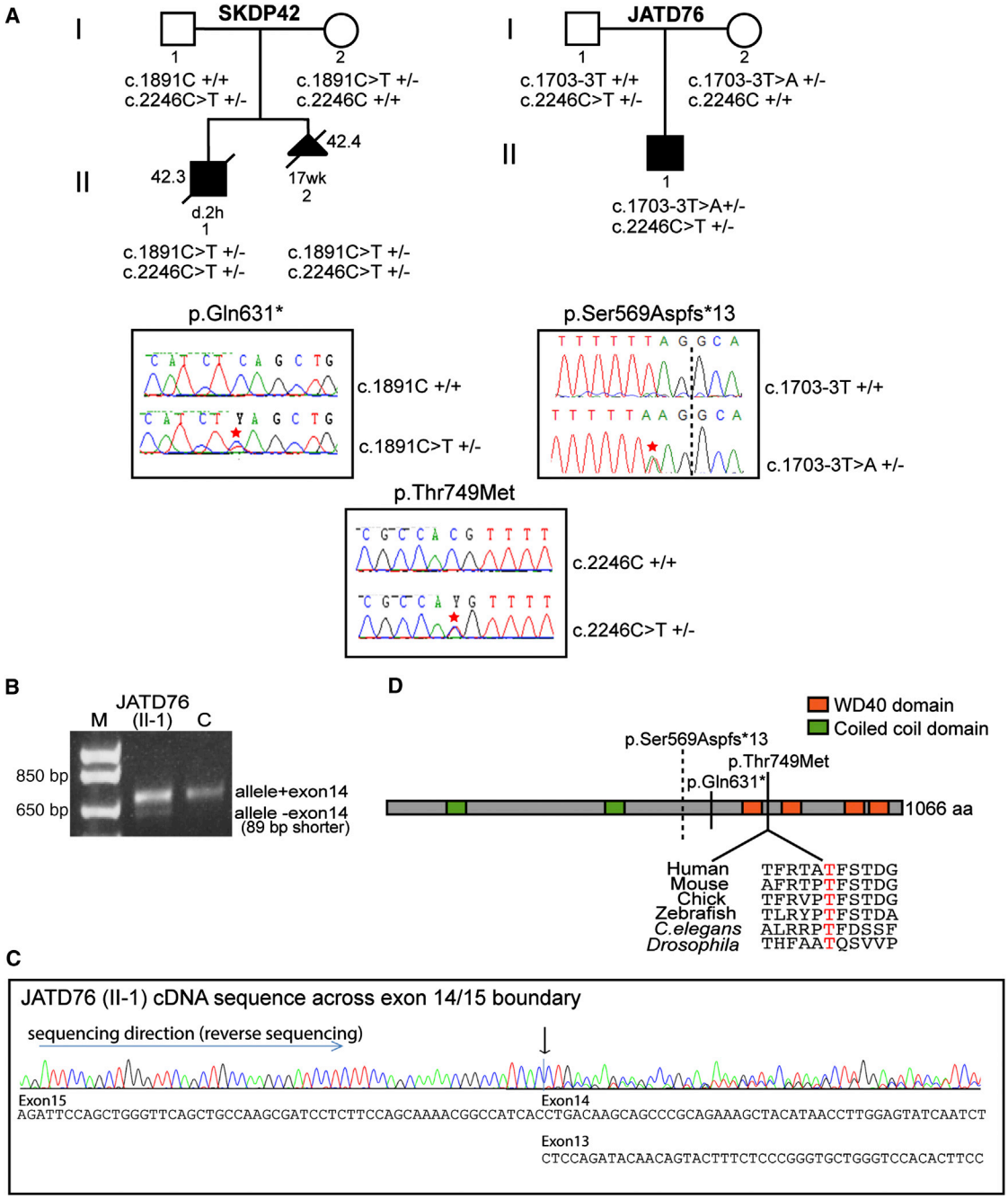

Figure 2. Segregation of *WDR60* Variants and the Predicted Effect on Protein

(A) Pedigree structure and *WDR60* genotypes for the Australian SRPS family (SKDP42: individual II-1 = SKDP42.3; II-2 = SKDP42.4) and the Spanish Jeune syndrome family (JATD76). Sequencing chromatograms of genomic DNA show examples of each of the *WDR60* mutations. Asterisks mark mutated base; dotted line in JATD76 sequence marks the intron 13/exon 14 junction.

(B) Agarose gel showing RT-PCR products amplified from the proband in family JATD76 (II-1) and control cDNA, using primers in exon 13 and 18, spanning the splice mutation predicted to result in skipping of exon 14 (see Figure S1 for schema). Abbreviations are as follows: M, marker; C, control.

(C) Sequencing chromatogram of the JATD76 (II-1) cDNA sample showing the nondeleted (upper line) and exon-14-skipped (lower line) alleles. Arrow indicates exon 15 boundary with exon 14 (control allele) or 13 (mutated allele). Note the sequencing shown is in the reverse orientation. Primer sequences available on request.

(D) Schematic of human WDR60 showing the main protein domains and the positions of the residues affected by the three mutations found in this study. The residue altered by the c.2246C>T (p.Thr749Met) missense mutation present in both families is conserved back to *Drosophila*. (Human ENST00000407559; Mouse ENSMUSG00000042050; Chicken ENSGALG00000006558; Zebrafish ENSDART00000109166; *C. elegans* c27F2.1; *Drosophila* FBgn0034095.)

coverage for SNP calling: >10-fold for homozygous SNPs, >15-fold for heterozygous SNPs). Additionally, we used variants that passed GATK Variant Quality Score Recalibration. Remaining SNPs and indels were assessed according to prediction of potentially damaging consequence ("nonsynonymous SNV," "splicing," "frameshift substitution," "stopgain SNV," "stoploss SNV") by using both RefSeq and UCSC transcripts. Further filtering excluded SNPs with a minor allele frequency (MAF) > 0.001 observed in NCBI dbSNP (release 135), 1000 Genomes,[29] 1000 Genomes small indels (called with the DINDEL program[30]), the SNPs of 46Genomes release by Complete Genomics, and other whole exomes from more than 1,200 control samples run internally by similar capture technology. Variants not present in any of these databases were considered novel.

Given that SRPS is known to follow a recessive mode of inheritance, compound heterozygosity was considered most likely in this nonconsanguineous family. We therefore analyzed the data for heterozygous carriage of at least two rare (either novel or MAF < 0.001) nonsynonymous SNPs or indels in the same gene, both carried by the affected individual. After quality-filtering as described, two genes remained with compound heterozygosity for either novel or rare SNPs: *WDR60* and *CILP* (MIM 603489). The data were also analyzed for homozygosity of novel or rare SNPs (MAF < 0.001); no genes were identified by this analysis (see Table S2 available online for summary of identified variants).

The compound heterozygous *WDR60* variants identified in individual SKDP42.3 (II-1 in Figure 2A) are both novel. One, in exon 15 (c.1891C>T [p.Gln631*]; RefSeq accession number NM_018051.4), introduces a stop codon in a highly conserved region (GERP [Genomic Evolutionary Rate Profiling][31] score 4.15). The other, in exon 17 (c.2246C>T [p.Thr749Met]), is a nonsynonymous variant also found in a highly conserved region (GERP score 5.04). The function prediction algorithms PolyPhen,[32] MutationTaster, and SIFT[33] predicted the nonsynonymous variant to be "probably damaging" (0.999), "disease-causing," and "deleterious," respectively. Sanger sequencing demonstrated appropriate segregation of these mutations in the parents and other affected individual in this family (Figure 2A). Although rare (MAF < 0.0005) compound heterozygous mutations were also found in *CILP*, neither were novel, both were predicted to be benign and tolerated by PolyPhen and SIFT, and Sanger sequencing showed that they did not segregate appropriately in the family and thus could not be causative.

Thus, mutations in *WDR60* were considered the most likely cause of disease in the Australian family. In support of this we reviewed the exome sequencing data of *WDR60* from 1,985 unrelated individuals. A total of 152 SNPs and indels were identified, 87 of which had MAF < 0.005; of these 28 were in coding regions (including splice sites), and 25 passed quality control. No individual was a compound heterozygote for mutations in *WDR60*, suggesting that the probability of finding compound heterozygous *WDR60* mutations randomly in the human population is low. However, to further support causality of these mutations, we interrogated exome sequencing data from an additional 54 individuals with skeletal ciliopathies, primarily Jeune syndrome. All samples were obtained with approval of the relevant ethical and licensing authorities; in the United Kingdom, this was the UCL-ICH/Great Ormond St. Hospital Research Ethics Committee (#08/H0713/82).

For these exomes, library preparation, sequencing, alignment, and calling was performed largely as per the Australian family, with details as previously described.[20] Exome variant profiles were filtered by EVAR software tool v.0.2.2 beta. After filtering against 75 control exomes from the UK10K project, remaining variants were filtered for MAF < 0.005 in dbSNP (release 137), 1000 Genomes, and the NHLBI Exome Sequencing Project, then filtered by a quality score implicating a base error rate <0.1%. Intronic variants within 12 bp of an intron/exon boundary and coding nonsynonymous variants (missense, nonsense, and frameshifts) were retained. Finally, any genes with biallelic variants with MAF > 0.005 in 500 control exomes available via the UK10K project were removed, and remaining candidate genes were checked for their presence in the cilia proteome as a means of prioritization (see Table S3 for summary of filtering steps and identified variants).

After filtering according to these criteria, one of the 54 individuals (JATD76, II-1 in Figure 2A) was found to carry two potentially damaging heterozygous mutations in *WDR60*. One of these is the same novel missense change carried by the Australian family (c.2246C>T [p.Thr749Met]). The other is a novel point mutation in intron 13 within the conserved exon 14 splice acceptor site and was therefore predicted to affect splicing of exon 14 (g.158706921T>A [c.1703−3T>A]). This was confirmed by qRT-PCR and sequencing of cDNA prepared from a fibroblast cell line derived from individual JATD76 (II-1) (Figures 2B, 2C, and S1). This showed that exon 14 was removed by aberrant splicing, resulting in a frameshift, leading to premature termination of the resultant protein (p.Ser569Aspfs*13). Both *WDR60* mutations were shown by Sanger sequencing to segregate appropriately in this family (Figure 2A).

Individual JATD76 (II-1) also carried compound heterozygous variants in *TTN* (MIM 188840) and a homozygous change in *LAMA5* (MIM 601033). With respect to *LAMA5*, a homozygous model of inheritance for an extremely rare SNP was considered unlikely in the absence of a history of consanguinity in this family; further, the observed variant (c.6982G>A [p.Ala2328Thr]; RefSeq NM_005560.3) was predicted to affect a nonconserved residue (GERP score 0.34) and is likely to be "benign," "a polymorphism," or "tolerated" according to PolyPhen2, MutationTaster, and SIFT. Finally, although *Lama5* mutant mice do display polycystic kidney disease and neural tube closure defects, they show no reported signs of the skeletal defects that characterize Jeune syndrome.[34] Although the variants in

TTN affected highly conserved amino acids (GERP scores >4), PolyPhen2, MutationTaster, and SIFT differed as to their predicted effect. Although one (c.6950G>A [p.Arg2317His]; RefSeq NM_133378.4) was predicted to be "probably damaging," "disease-causing," and "deleterious" by these programs, respectively, the other (c.7611A>T [p.Arg2537Ser]) was predicted to be a benign polymorphism by Polyphen2 and MutationTaster, although SIFT predicted deleterious effects. However, *TTN* was excluded because exome sequencing commonly reveals mutations in this gene, probably because of its large size (M.S., A.M.M.-L., E.L.D.; unpublished observation). Furthermore, variants in *TTN* cause myopathy in humans (MIM 608807, MIM 611705, MIM 603689), inconsistent with the Jeune syndrome phenotype in this individual.

The affected individual JATD76 (II-1) is the first child of healthy nonconsanguineous Spanish parents. Prenatal ultrasound at 20–21 weeks' gestation detected short femora. Delivery was uneventful at 41 weeks' gestation (birth weight 3,170 g, 25th–50th centile; length at birth 49 cm, 50th centile; and head circumference at birth 36 cm, 75th–90th centile). At birth he presented with a narrow chest, preaxial polydactyly on the right hand (extra digit subsequently removed by surgery), and a small clinically insignificant ventricular septal defect (Figures 1C–1F). At age 1 year he showed signs of failure to thrive (weight 6,640 g, <3rd centile; length 69 cm, 3rd centile), and at age 5 years and 3 months remained on the lower extreme of the growth charts (weight 14.5 kg, 5th centile; height 101 cm, 1st centile). He has no evidence of renal, hepatic, retinal, neurological, or developmental problems to date (now aged 5 years). Compared to the Australian SRPS family, this represents a relatively mild clinical course.

Because both families in this study share one missense mutation (c.2246C>T [p.Thr749Met]), and given Australia's recent migrant history, we investigated whether this variant could represent a founder effect. The genotype likelihoods for the variants were used to phase the data via the software BEAGLE 3.3.2; subsequent association analysis was performed with the BEAGLE Utilities program Cluster2haps, which identifies haplotype clusters by testing the allele sequences for association with the trait status; results are reported as p values. The *WDR60* gene region for the cohort and control samples was also analyzed with the R package hapFabia, which identifies short identity-by-descent (IBD) segments in large sequencing data. No significant shared haplotypes were identified by either approach, excluding a common founder effect in these two families (data not shown).

Sanger sequencing analysis for the three identified *WDR60* mutations in 55 additional Jeune syndrome samples with insufficient DNA for whole-exome sequencing did not reveal any further cases. Because of the length of *WDR60*, we have not sequenced the remaining exons of *WDR60* in these individuals.

WDR60 is a relatively uncharacterized evolutionarily conserved protein predicted to contain four WD40 repeat domains and two coiled-coil domains. These domains have been implicated in protein-protein interactions, and WD40 repeats in particular are highly represented in proteins involved in IFT and cilia function.[9] The c.1891C>T mutation in family SKDP42 and the c.1703−3T>A mutation in family JATD76 are both predicted to lead to truncation of the protein after the coiled-coiled domains but prior to the WD40 repeats (p.Gln631* and p.Ser569Aspfs*13, respectively); the c.2246C>T missense mutation in both families is predicted to lead to an amino acid substitution within the run of WD40 repeat sequences (p.Thr749Met; Figure 2D). In addition, the relative intensity of the mutant JATD76 splice allele versus wild-type allele by RT-PCR analysis (Figure 2B) suggests that this mutant allele is subject to some level of nonsense-mediated decay. In short, all mutations are likely to result in loss or alteration to the WD40 functional domains or loss of protein.

As is the case in general for ciliopathies,[35] different mutations in the same gene can lead to distinct skeletal ciliopathies with, for example, *DYNC2H1* mutations found in both Jeune syndrome and SRPS type III.[16] Furthermore, we have previously described significant phenotypic variability among Jeune syndrome individuals with *DYNC2H1* mutations, including between siblings of identical *DYNC2H1* genotype.[21] Consistent with this, there is a marked difference in phenotypic severity between individuals in the families in this study. Both families share a common missense mutation, and the other mutation in both cases is predicted to introduce a premature stop codon. These protein-truncating alleles may result in nonsense-mediated mRNA decay or encode a nonfunctional truncated protein, although production of a protein fragment with some function cannot be ruled out. It is therefore possible that differences in phenotypic severity may not result from *WDR60* genotype alone, but rather may reflect the effect of genetic modifying alleles, a phenomenon that has also been well documented for ciliopathies,[35] and/or epigenetic, environmental, or stochastic effects.

Although WDR60 is relatively uncharacterized, two recent proteomic analyses of cilia in mouse inner medullary collecting duct (IMCD3) cells[36] and in multiciliated mouse tracheal epithelial cells[37] identified this protein, suggesting that it may have a function in the core processes of ciliogenesis relevant to both primary and motile cilia. In addition, functional genomics analyses of cilia in *C. elegans* identified the WDR60 ortholog C27F2.1, and this protein appears in the online ciliome, strongly suggesting a conserved function for WDR60 at the cilium.[38] In support of this, one of these studies showed localization of exogenously expressed WDR60 at the cilium in IMCD3 cells.[36] We have now shown by using a commercially available antibody that endogenous WDR60 localizes in a diffuse pattern at the base of the primary cilium in cultured immortalized C-28/I2 human chondrocytes (Figures 3A–3E).

We next analyzed primary fibroblasts derived from the three individuals with *WDR60* mutations to determine the proportion of ciliated cells in cultures induced to

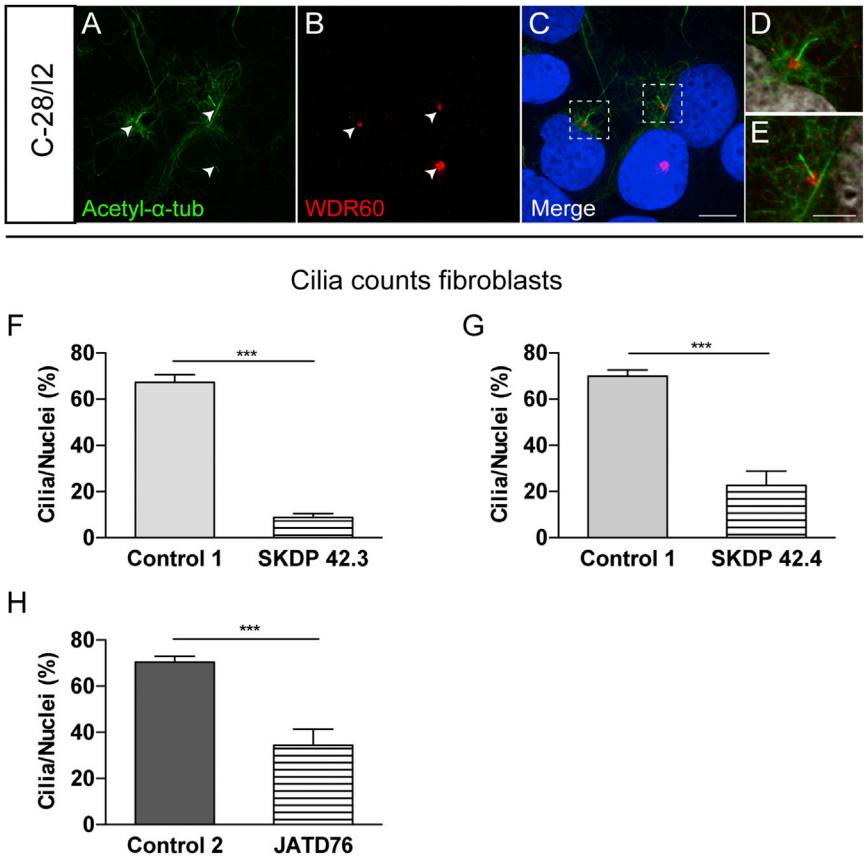

Figure 3. WDR60 Localizes to the Base of the Cilium in Human Chondrocytes and Ciliogenesis Is Impaired in Fibroblast Cultures from Affected Individuals

(A–E) C-28/I2 immortalized human chondrocytes were serum starved for 24 hr in DMEM+0.2% FBS prior to fixing in 4% paraformaldehyde (PFA). Cells were stained with antibodies to acetylated α-tubulin (green) and WDR60 (red), showing localization of WDR60 at the base of the cilium (marked with arrowheads in A and B; see Table S4 for details of antibodies used). Nuclei were stained with 4′,6-Diamidino-2-Phenylindole (DAPI; blue). Cells were imaged on an Olympus Deltavision IX71 inverted microscope with a 100× objective. High-power images of boxed regions in (C) shown in (D) and (E). Scale bars represent 10 μm in (A)–(C) and 5 μm in (D) and (E).

(F–H) Graphs showing a decreased percentage of ciliated cells in fibroblasts prepared from affected individuals SKDP42.3 (F), SKDP42.4 (G), and JATD76 (II-1; H) versus control fibroblast lines from postnatal foreskin (F, G) or adult skin (H). Cells were cultured for a maximum of six passages and serum starved and fixed as above. Acetylated α-tubulin-stained cilia were counted manually and expressed as a percentage of the number of nuclei. Data shown are from a minimum of three independent experiments. For each experiment at least 100 cells were counted, the mean percentage of ciliated cells was calculated, and the mean values compared statistically by a Student's t test (***$p < 0.0001$) with Prism 5 (Graphpad) software. Error bars represent standard error of the mean (SEM).

produce cilia by serum starvation (see legend to Figure 3 for experimental details). Controls were fibroblasts from postnatal foreskin (PromoCell, for SKDP42 analysis) or adult skin (ECACC, for JATD76 analysis). These are optimal controls for individuals SKDP42.3 (died at 2 hr postnatally) and JATD76 (II-1; fibroblasts collected at age 5 years). The postnatal control line was considered closest to the fetal fibroblasts collected from SKDP42.4. Regardless, both control cultures (as well as an additional postnatal control we analyzed) showed a comparable cilia/nuclei ratio of approximately 70%, suggesting that the ability of fibroblasts to form cilia is not dependent on the age of collection. The percentage of ciliated cells was drastically reduced in SKDP42.3 cells (Figure 3F). Likewise, a significant, although less marked, reduction in the percentage of ciliated cells was also observed in the SKDP42.4 and JATD76 cultures (Figures 3G and 3H). In the minor percentage of mutant cells with a detectable cilium, there was no obvious difference in length compared to control cells. However, to check that stunted cilia were not masked by the cytoplasmic microtubule network detected by acetylated α-tubulin, used to mark the axoneme in these experiments, we further quantified ciliated cells in SKDP42.3 cultures after staining of the axoneme with the Arf-like small GTPase ARL13b. This confirmed reduced frequency of readily detectable cilia, consistent with the acetylated α-tubulin data (Figure S2). Taken together, these data suggest a defect in ciliogenesis in these individuals and potentially link WDR60 to this process.

Because skeletal ciliopathies have been linked primarily to mutations in IFT genes, we next analyzed localization of key IFT proteins by immunofluorescence analysis in serum-starved SKDP42.3 cells. In control fibroblasts, the IFT-A protein IFT144 and the IFT-B protein IFT88 are localized at the transition zone, which lies between the basal body and axoneme, and less prominently along the axoneme (Figures 4A and 4D). In the small percentage of SKDP42.3 ciliated cells, the normal distribution of both of these proteins was essentially maintained (Figures 4C and 4F). However, in those mutant cells that appear to lack a primary cilium, both IFT144 (Figure 4B) and IFT88 (Figure 4E) accumulated at the centrosome or basal body (as marked by γ-tubulin).

These data are consistent with findings in MEFs derived from mouse mutants that lack cilia because of defects in anterograde IFT, including *Kif3a* and *Ift172* mutant mice, suggesting that IFT proteins, which are required for axonemal extension, can be recruited to the basal body even under conditions where cilium assembly is inhibited.[39] IFT88 in particular has previously been reported to be a centrosomal protein,[40] so we next sought to characterize localization of a noncentrosomal protein. For this we

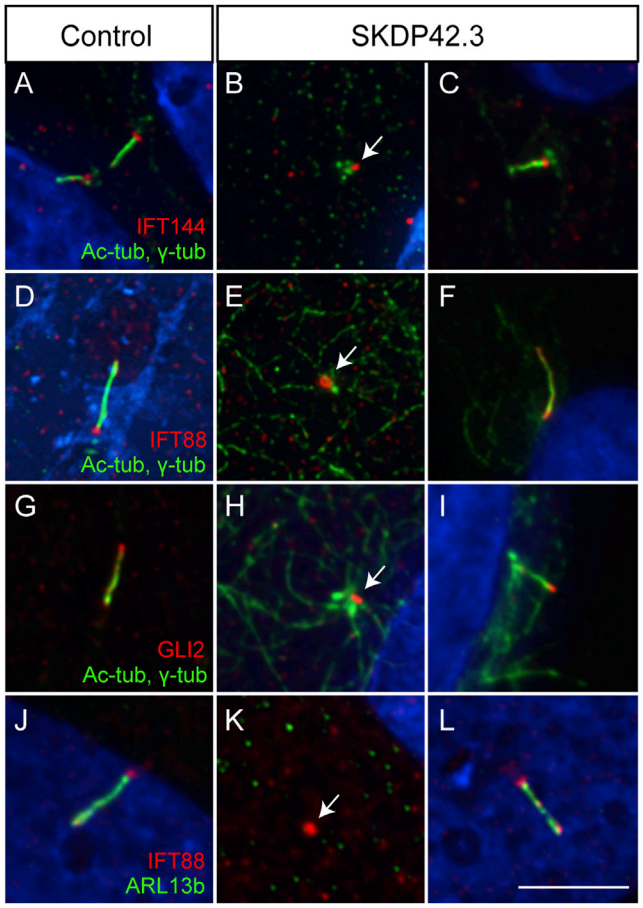

Figure 4. Localization of IFT and Trafficking Proteins in *WDR60* Mutant Fibroblasts

Fibroblasts from individual SKDP42.3 and control fibroblast lines were serum starved as described (see legend to Figure 3), fixed, and stained for (A–C) IFT144 (red), (D–F; J–L) IFT88 (red), (G–I) GLI2 (red), and (J–L) ARL13b (green). In (A)–(I), cells were costained for acetylated α-tubulin and γ-tubulin (green). Nuclei were stained with DAPI (blue), indicating that in (A) two independent cells are shown. Localization in cells in the mutant cultures that don't form a detectable primary cilium are shown in (B), (E), (H), and (K). Arrows point to accumulated proteins. In those mutant cells that form a cilium, all proteins analyzed show a similar localization to control cells as shown in (C), (F), (I), and (L). For IFT144 experiments (A–C) only, cells were treated with saponin (0.05% in PBS) for 1 min prior to fixation in 4% PFA for 10 min. In (D)–(I), cells were fixed in ice-cold MeOH for 5 min, in (J)–(L) in 4% PFA. Cells were imaged on an Olympus Deltavision IX71 inverted microscope with a 100× objective. Scale bars represent 5 μm. See Table S4 for details of antibodies used.

used GLI2, which is a transcriptional mediator of hedgehog signaling and shuttles in and out of the cilium in response to stimulation of the hedgehog pathway.[41] Under basal conditions in ciliated cells, GLI2 normally localizes primarily to the tip of the cilium (Figure 4G), with further enrichment at this localization upon treatment of hedgehog-responsive cells with the hedgehog agonist SAG.[10] Those SKDP42.3 cells that possessed a cilium essentially displayed the wild-type localization of GLI2 (Figure 4I). However, in apparently nonciliated SKDP42.3 cells, we saw a striking accumulation of GLI2 close to the γ-tubulin staining domain, irrespective of whether they had been stimulated with SAG (Figure 4H, non-SAG-treated cells shown only). Because GLI2 is not normally localized to the centrosome, these data raise the possibility that in *WDR60* mutant cells, the mother centriole migrates to the membrane and initiates basal body maturation but fails to extend an axoneme. Alternatively, a drastically truncated axoneme not detectable by immunofluorescence analysis may be present in these cells.

Mouse embryonic fibroblasts (MEFs) from embryos null for *Ift144* produce very stunted cilia undetectable by acetylated α-tubulin resulting from the virtual absence of microtubules within the axoneme.[10] We therefore analyzed ARL13b localization as an independent marker of the axoneme, along with IFT88, which in *Ift144*-null MEFs marks the cilium even in the absence of microtubules. ARL13b localizes along the axoneme in both control and ciliated SKDP42.3 cells (Figures 4J and 4L). However, in those mutant cells with no obvious cilium, ARL13b does not accumulate with IFT88 at the basal body (Figure 4K), and there is no evidence of widespread stunted cilia with either marker, at least at this level of detection. Taken together, these data suggest that like IFT proteins, GLI2 can be recruited to the basal body in the absence of an obvious axonemal extension, whereas ARL13b recruitment probably occurs at a later stage in ciliogenesis and/or by a different mechanism. This is consistent with *Ift144*-null MEFs where GLI2 is present in the stunted cilia, whereas ARL13b is not detectable.[10] Furthermore, the fact that some SKDP42.3 cells are able to form cilia with apparently normal structural and trafficking properties suggests that a threshold level of a WDR60-mediated function may be required in a given cell at a specific time to allow ciliogenesis.

In summary, by using whole-exome sequencing, initially in only one individual, we found novel mutations in *WDR60* in an Australian family with SRPS type III and in a Spanish family with Jeune syndrome. Although both families share one disease allele, haplotype analysis suggests no shared ancestry. The varying phenotypic severity caused by mutations in the same gene may be due to differing effects of the second mutation on protein function but, consistent with other ciliopathy cases, it may also reflect differences in the genomic architecture or epigenetic or other nongenetic factors in each affected individual. By using fibroblast lines from affected individuals, we have shown a defect in ciliogenesis, possibly related to failure in IFT-dependent axonemal extension. Given the connection to IFT in the skeletal ciliopathies solved to date, future work will explore the function of WDR60 and its possible role in regulating this specialized trafficking process.

Supplemental Data

Supplemental Data include two figures and four tables and can be found with this article online at http://www.cell.com/AJHG/.

Acknowledgments

The authors would like to thank the families for their cooperation and interest in the study. We also wish to thank Carlos Vázquez (Unidad de Fibrosis Quística y Neumologia Pediatrica, Hospital Universitario Cruces, Baracaldo, Spain) for referring family JATD76, Linda Bradbury for collecting initial samples from family SKDP-42, Gael Phillips (Pathology Queensland) for the autopsy report on individual SKDP42.4, Thor Friis (QUT) for providing the C-28/I2 cell line, Sharon Song, Marina Doskoi, and Maria Rondon for technical support, and Kelly Smith for helpful discussion. All confocal microscopy was carried out at the Institute for Molecular Bioscience Dynamic Imaging Facility for Cancer Biology, developed with the generous support of the Australian Cancer Research Foundation. C.R.C. is the recipient of a UQ International PhD Scholarship, and C.W. was an Australian National Health and Medical Research Council (NHMRC) Senior Research Fellow. M.A.B. was funded by an NHMRC Senior Principal Research Fellowship, and support was also received from the Rebecca Cooper Medical Research Foundation. P.L.B. is a Wellcome Trust Senior Research Fellow and received funding from the EU FP-7 framework programme (SYSCILIA grant). P.L.B. and M.S. acknowledge funding from the Dutch Kidney Foundation (CP 11.18). P.J.S. is supported by the Wellcome Trust and British Heart Foundation. H.M.M. received funds from Action Medical Research UK, Newlife Foundation for Disabled Children UK, and the Henry Smith Charity UK. M.S. is funded by an Action Medical Research UK Clinical Training Fellowship (RTF-1411). This publication used sequencing data generated by the UK10K project, which is funded by Wellcome Trust UK (award WT091310). A list of UK10K contributors can be found at http://www.uk10k.org.

Received: March 16, 2013
Revised: May 10, 2013
Accepted: June 27, 2013
Published: August 1, 2013

Web Resources

The URLs for data presented herein are as follows:

1000 Genomes, http://browser.1000genomes.org
BEAGLE, http://faculty.washington.edu/browning/beagle/beagle.html
CASAVA, http://www.illumina.com/software/genome_analyzer_software.ilmn
Cilia proteome, http://www.ciliaproteome.org
Complete Genomics, http://www.completegenomics.com/sequence-data/download-data/
dbSNP, http://www.ncbi.nlm.nih.gov/projects/SNP/
FEVA (Family-Based Exome Variants Analysis), http://www.exome.info
GATK, http://www.broadinstitute.org/gatk/
hapFabia, http://www.bioconductor.org/packages/2.11/bioc/html/hapFabia.html
MutationTaster, http://www.mutationtaster.org/
NHLBI Exome Sequencing Project (ESP) Exome Variant Server, http://evs.gs.washington.edu/EVS/
Novoalign, http://www.novocraft.com/main/page.php?s=novoalign
Online Mendelian Inheritance in Man (OMIM), http://www.omim.org/
Picard, http://picard.sourceforge.net/
PolyPhen-2, http://www.genetics.bwh.harvard.edu/pph2/
RefSeq, http://www.ncbi.nlm.nih.gov/RefSeq
SIFT, http://sift.bii.a-star.edu.sg/
UCSC Genome Browser, http://genome.ucsc.edu
UK10K Consortium, http://www.uk10k.org/
UniProt, http://www.uniprot.org/

References

1. Waters, A.M., and Beales, P.L. (2011). Ciliopathies: an expanding disease spectrum. Pediatr. Nephrol. *26*, 1039–1056.
2. Hildebrandt, F., Benzing, T., and Katsanis, N. (2011). Ciliopathies. N. Engl. J. Med. *364*, 1533–1543.
3. Lee, J.E., and Gleeson, J.G. (2011). A systems-biology approach to understanding the ciliopathy disorders. Genome Med. *3*, 59–67.
4. Huangfu, D., Liu, A., Rakeman, A.S., Murcia, N.S., Niswander, L., and Anderson, K.V. (2003). Hedgehog signalling in the mouse requires intraflagellar transport proteins. Nature *426*, 83–87.
5. Warman, M.L., Cormier-Daire, V., Hall, C., Krakow, D., Lachman, R., LeMerrer, M., Mortier, G., Mundlos, S., Nishimura, G., Rimoin, D.L., et al. (2011). Nosology and classification of genetic skeletal disorders: 2010 revision. Am. J. Med. Genet. A. *155A*, 943–968.
6. Walczak-Sztulpa, J., Eggenschwiler, J., Osborn, D., Brown, D.A., Emma, F., Klingenberg, C., Hennekam, R.C., Torre, G., Garshasbi, M., Tzschach, A., et al. (2010). Cranioectodermal dysplasia, Sensenbrenner syndrome, is a ciliopathy caused by mutations in the IFT122 gene. Am. J. Hum. Genet. *86*, 949–956.
7. Huber, C., and Cormier-Daire, V. (2012). Ciliary disorder of the skeleton. Am. J. Med. Genet. C. Semin. Med. Genet. *160C*, 165–174.
8. Mill, P., Lockhart, P.J., Fitzpatrick, E., Mountford, H.S., Hall, E.A., Reijns, M.A., Keighren, M., Bahlo, M., Bromhead, C.J., Budd, P., et al. (2011). Human and mouse mutations in WDR35 cause short-rib polydactyly syndromes due to abnormal ciliogenesis. Am. J. Hum. Genet. *88*, 508–515.
9. Hao, L., and Scholey, J.M. (2009). Intraflagellar transport at a glance. J. Cell Sci. *122*, 889–892.
10. Liem, K.F., Jr., Ashe, A., He, M., Satir, P., Moran, J., Beier, D., Wicking, C., and Anderson, K.V. (2012). The IFT-A complex regulates Shh signaling through cilia structure and membrane protein trafficking. J. Cell Biol. *197*, 789–800.
11. Beales, P.L., Bland, E., Tobin, J.L., Bacchelli, C., Tuysuz, B., Hill, J., Rix, S., Pearson, C.G., Kai, M., Hartley, J., et al. (2007). IFT80, which encodes a conserved intraflagellar transport protein, is mutated in Jeune asphyxiating thoracic dystrophy. Nat. Genet. *39*, 727–729.
12. Cavalcanti, D.P., Huber, C., Sang, K.H., Baujat, G., Collins, F., Delezoide, A.L., Dagoneau, N., Le Merrer, M., Martinovic, J., Mello, M.F., et al. (2011). Mutation in IFT80 in a fetus with the phenotype of Verma-Naumoff provides molecular evidence for Jeune-Verma-Naumoff dysplasia spectrum. J. Med. Genet. *48*, 88–92.
13. Davis, E.E., Zhang, Q., Liu, Q., Diplas, B.H., Davey, L.M., Hartley, J., Stoetzel, C., Szymanska, K., Ramaswami, G., Logan, C.V., et al.; NISC Comparative Sequencing Program. (2011). TTC21B contributes both causal and modifying alleles across the ciliopathy spectrum. Nat. Genet. *43*, 189–196.

14. Bredrup, C., Saunier, S., Oud, M.M., Fiskerstrand, T., Hoischen, A., Brackman, D., Leh, S.M., Midtbø, M., Filhol, E., Bole-Feysot, C., et al. (2011). Ciliopathies with skeletal anomalies and renal insufficiency due to mutations in the IFT-A gene WDR19. Am. J. Hum. Genet. *89*, 634–643.
15. Perrault, I., Saunier, S., Hanein, S., Filhol, E., Bizet, A.A., Collins, F., Salih, M.A., Gerber, S., Delphin, N., Bigot, K., et al. (2012). Mainzer-Saldino syndrome is a ciliopathy caused by IFT140 mutations. Am. J. Hum. Genet. *90*, 864–870.
16. Dagoneau, N., Goulet, M., Geneviève, D., Sznajer, Y., Martinovic, J., Smithson, S., Huber, C., Baujat, G., Flori, E., Tecco, L., et al. (2009). DYNC2H1 mutations cause asphyxiating thoracic dystrophy and short rib-polydactyly syndrome, type III. Am. J. Hum. Genet. *84*, 706–711.
17. Hoffer, J.L., Fryssira, H., Konstantinidou, A.E., Ropers, H.H., and Tzschach, A. (2013). Novel WDR35 mutations in patients with cranioectodermal dysplasia (Sensenbrenner syndrome). Clin. Genet. *83*, 92–95.
18. Arts, H.H., Bongers, E.M., Mans, D.A., van Beersum, S.E., Oud, M.M., Bolat, E., Spruijt, L., Cornelissen, E.A., Schuurs-Hoeijmakers, J.H., de Leeuw, N., et al. (2011). C14ORF179 encoding IFT43 is mutated in Sensenbrenner syndrome. J. Med. Genet. *48*, 390–395.
19. Gilissen, C., Arts, H.H., Hoischen, A., Spruijt, L., Mans, D.A., Arts, P., van Lier, B., Steehouwer, M., van Reeuwijk, J., Kant, S.G., et al. (2010). Exome sequencing identifies WDR35 variants involved in Sensenbrenner syndrome. Am. J. Hum. Genet. *87*, 418–423.
20. Schmidts, M., Frank, V., Eisenberger, T., Al Turki, S., Bizet, A.A., Antony, D., Rix, S., Decker, C., Bachmann, N., Bald, M., et al. (2013). Combined NGS approaches identify mutations in the intraflagellar transport gene IFT140 in skeletal ciliopathies with early progressive kidney disease. Hum. Mutat. *34*, 714–724.
21. Schmidts, M., Arts, H.H., Bongers, E.M.H.F., Yap, Z., Oud, M.M., Antony, D., Duijkers, L., Emes, R.D., Stalker, J., Yntema, J.B., et al.; UK10K. (2013). Exome sequencing identifies DYNC2H1 mutations as a common cause of asphyxiating thoracic dystrophy (Jeune syndrome) without major polydactyly, renal or retinal involvement. J. Med. Genet. *50*, 309–323.
22. Thiel, C., Kessler, K., Giessl, A., Dimmler, A., Shalev, S.A., von der Haar, S., Zenker, M., Zahnleiter, D., Stöss, H., Beinder, E., et al. (2011). NEK1 mutations cause short-rib polydactyly syndrome type majewski. Am. J. Hum. Genet. *88*, 106–114.
23. Ruiz-Perez, V.L., Tompson, S.W., Blair, H.J., Espinoza-Valdez, C., Lapunzina, P., Silva, E.O., Hamel, B., Gibbs, J.L., Young, I.D., Wright, M.J., and Goodship, J.A. (2003). Mutations in two nonhomologous genes in a head-to-head configuration cause Ellis-van Creveld syndrome. Am. J. Hum. Genet. *72*, 728–732.
24. Li, H., and Homer, N. (2010). A survey of sequence alignment algorithms for next-generation sequencing. Brief. Bioinform. *11*, 473–483.
25. Li, H., Handsaker, B., Wysoker, A., Fennell, T., Ruan, J., Homer, N., Marth, G., Abecasis, G., and Durbin, R.; 1000 Genome Project Data Processing Subgroup. (2009). The Sequence Alignment/Map format and SAMtools. Bioinformatics *25*, 2078–2079.
26. McKenna, A., Hanna, M., Banks, E., Sivachenko, A., Cibulskis, K., Kernytsky, A., Garimella, K., Altshuler, D., Gabriel, S., Daly, M., and DePristo, M.A. (2010). The Genome Analysis Toolkit: a MapReduce framework for analyzing next-generation DNA sequencing data. Genome Res. *20*, 1297–1303.
27. DePristo, M.A., Banks, E., Poplin, R., Garimella, K.V., Maguire, J.R., Hartl, C., Philippakis, A.A., del Angel, G., Rivas, M.A., Hanna, M., et al. (2011). A framework for variation discovery and genotyping using next-generation DNA sequencing data. Nat. Genet. *43*, 491–498.
28. Wang, K., Li, M., and Hakonarson, H. (2010). ANNOVAR: functional annotation of genetic variants from high-throughput sequencing data. Nucleic Acids Res. *38*, e164.
29. Abecasis, G.R., Altshuler, D., Auton, A., Brooks, L.D., Durbin, R.M., Gibbs, R.A., Hurles, M.E., and McVean, G.A.; 1000 Genomes Project Consortium. (2010). A map of human genome variation from population-scale sequencing. Nature *467*, 1061–1073.
30. Albers, C.A., Lunter, G., MacArthur, D.G., McVean, G., Ouwehand, W.H., and Durbin, R. (2011). Dindel: accurate indel calls from short-read data. Genome Res. *21*, 961–973.
31. Cooper, G.M., Goode, D.L., Ng, S.B., Sidow, A., Bamshad, M.J., Shendure, J., and Nickerson, D.A. (2010). Single-nucleotide evolutionary constraint scores highlight disease-causing mutations. Nat. Methods *7*, 250–251.
32. Adzhubei, I.A., Schmidt, S., Peshkin, L., Ramensky, V.E., Gerasimova, A., Bork, P., Kondrashov, A.S., and Sunyaev, S.R. (2010). A method and server for predicting damaging missense mutations. Nat. Methods *7*, 248–249.
33. Kumar, P., Henikoff, S., and Ng, P.C. (2009). Predicting the effects of coding non-synonymous variants on protein function using the SIFT algorithm. Nat. Protoc. *4*, 1073–1081.
34. Gao, J., DeRouen, M.C., Chen, C.H., Nguyen, M., Nguyen, N.T., Ido, H., Harada, K., Sekiguchi, K., Morgan, B.A., Miner, J.H., et al. (2008). Laminin-511 is an epithelial message promoting dermal papilla development and function during early hair morphogenesis. Genes Dev. *22*, 2111–2124.
35. Novarino, G., Akizu, N., and Gleeson, J.G. (2011). Modeling human disease in humans: the ciliopathies. Cell *147*, 70–79.
36. Ishikawa, H., Thompson, J., Yates, J.R., 3rd, and Marshall, W.F. (2012). Proteomic analysis of mammalian primary cilia. Curr. Biol. *22*, 414–419.
37. Hoh, R.A., Stowe, T.R., Turk, E., and Stearns, T. (2012). Transcriptional program of ciliated epithelial cells reveals new cilium and centrosome components and links to human disease. PLoS ONE *7*, e52166.
38. Blacque, O.E., Perens, E.A., Boroevich, K.A., Inglis, P.N., Li, C., Warner, A., Khattra, J., Holt, R.A., Ou, G., Mah, A.K., et al. (2005). Functional genomics of the cilium, a sensory organelle. Curr. Biol. *15*, 935–941.
39. Goetz, S.C., Liem, K.F., Jr., and Anderson, K.V. (2012). The spinocerebellar ataxia-associated gene Tau tubulin kinase 2 controls the initiation of ciliogenesis. Cell *151*, 847–858.
40. Robert, A., Margall-Ducos, G., Guidotti, J.E., Brégerie, O., Celati, C., Bréchot, C., and Desdouets, C. (2007). The intraflagellar transport component IFT88/polaris is a centrosomal protein regulating G1-S transition in non-ciliated cells. J. Cell Sci. *120*, 628–637.
41. Kim, J., Kato, M., and Beachy, P.A. (2009). Gli2 trafficking links Hedgehog-dependent activation of Smoothened in the primary cilium to transcriptional activation in the nucleus. Proc. Natl. Acad. Sci. USA *106*, 21666–21671.